Atmos. Chem. Phys. Discuss., 13, 31041–31078, 2013
www.atmos-chem-phys-discuss.net/13/31041/2013/
doi:10.5194/acpd-13-31041-2013

Atmospheric Chemistry and Physics Discussions

Cloud condensation nucleus activity comparison of dry- and wet-generated mineral dust aerosol: the significance of soluble material

S. Garimella[1], **Y.-w. Huang**[1], **J. S. Seewald**[2], **and D. J. Cziczo**[1]

[1]Department of Earth, Atmospheric and Planetary Sciences, Massachusetts Institute of Technology, Cambridge, MA, USA
[2]Woods Hole Oceanographic Institution, Woods Hole, MA, USA

Received: 29 October 2013 – Accepted: 12 November 2013 – Published: 27 November 2013

Correspondence to: D. J. Cziczo (djcziczo@mit.edu)

Published by Copernicus Publications on behalf of the European Geosciences Union.

Abstract

This study examines the interaction of clay mineral particles and water vapor to determine the conditions required for cloud droplet formation. Droplet formation conditions are investigated for three clay minerals: illite, sodium-rich montmorillonite, and Arizona Test Dust. Using wet and dry particle generation coupled to a differential mobility analyzer (DMA) and cloud condensation nuclei counter, the critical activation of the clay mineral particles as cloud condensation nuclei is characterized. Electron microscopy (EM) is used to determine non-sphericity in particle shape. EM is also used to determine particle surface area and account for transmission of multiply charged particles by the DMA. Single particle mass spectrometry and ion chromatography are used to investigate soluble material in wet-generated samples and demonstrate that wet and dry generation yield compositionally different particles. Activation results are analyzed in the context of both κ-Köhler theory and Frenkel, Halsey, and Hill (FHH) adsorption activation theory. This study has two main results: (1) κ-Köhler is a suitable framework, less complex than FHH theory, to describe clay mineral nucleation activity despite apparent differences in κ with respect to size. For dry-generated particles the size dependence is likely an artifact of the shape of the size distribution: there is a sharp drop-off in particle concentration at ~300 nm, and a large fraction of particles classified with a mobility diameter less than ~300 nm are actually multiply charged, resulting in a much lower critical supersaturation for droplet activation than expected. For wet-generated particles, deviation from κ-Köhler theory is likely a result of the dissolution and redistribution of soluble material. (2) Wet-generation is found to be unsuitable for simulating the lofting of fresh dry dust because it changes the size-dependent critical supersaturations by fractionating and re-partitioning soluble material.

ACPD
13, 31041–31078, 2013

1 Introduction

Atmospheric aerosols play a significant role in the Earth's climate system, especially in the radiative budget and the hydrological cycle. Their influence on climate is via the so-called direct and indirect radiative forcing effects (Denman and Brasseur, 2007). The direct effect of aerosols on atmospheric radiation is through the scattering and absorption of light in both the shortwave and longwave regimes (Seinfeld and Pandis, 2006; Yu, et al., 2006; Christopher et al., 2009). This interaction with radiation depends on optical properties that vary significantly among different aerosols and depend on the wavelength of incoming radiation, relative humidity, aerosol concentration, spatial distribution, and atmospheric dynamics (Seinfeld and Pandis, 2006; Yu, et al., 2006; Christopher et al., 2009). Aerosols indirectly affect climate via their role in the formation and persistence of clouds in the atmosphere (Denman and Brasseur, 2007). As the availability and characteristics of aerosol particles vary, so do the formation, appearance, and persistence of clouds, which play a significant role in the climate system (Bergstrom et al., 2010; Logan et al., 2010; Lyapustin et al., 2010; Brock et al., 2011; Hansen et al., 2011; Lambe et al., 2011; McFarquhar et al., 2011; Booth et al., 2012).

In Earth's atmosphere, the condensation of water vapor into liquid droplets does not occur in the absence of aerosol particles. These particles, which provide a surface onto which the water vapor can condense, are called cloud condensation nuclei (CCN) because they facilitate the nucleation of droplets. Overall, the interaction of particulate matter and water vapor in the atmosphere is important for examining precipitation, cloud coverage, cloud persistence, and radiative forcing (Twomey, 1977; Albrecht, 1989; Forster and Ramaswamy, 2007).

According to the International Panel on Climate Change 4th Assessment Report, scientific understanding of most aerosol indirect effects on clouds and precipitation is considered "very low" (Denman and Brasseur, 2007). Since clouds are a significant factor in Earth's radiative budget, it is important to understand how aerosol particles serve as CCN and influence the formation and persistence of various types of clouds.

ACPD
13, 31041–31078, 2013

Aerosol particle size, chemical composition, mixing state, and ambient environment are all factors thought to influence CCN activity and are therefore of significant interest (Forster and Ramaswamy, 2007).

Field observations of aerosol particles indicate that they have variable size distributions and can be composed of organic material, inorganic material, or a mixture of both, e.g. (Shaw and Paur, 1983; Noble and Prather, 1996; Middlebrook et al., 1997; Dusek et al., 2006; Chou et al., 2008; Zhang et al., 2012). Therefore, laboratory studies of aerosol particles are necessary to determine how their various physical and chemical properties affect their ability to act as CCN in the atmosphere. Many previous studies investigated the nucleation potential both of individual types of aerosol particles (Raymond and Pandis, 2002, 2003; Petters and Kreidenweis, 2007; Koehler et al., 2009; Sullivan et al., 2009; Kumar et al., 2011a, b), and of simple mixtures (Raymond and Pandis, 2002, 2003; Bilde and Svenningsson, 2004; Abbatt et al., 2005). Observations indicate that the size of an aerosol particle is the primary factor in determining its efficiency as a CCN (Dusek et al., 2006), but its composition, though a secondary factor, should also be considered because it can affect how the particle will change due to the chemical interactions with its surroundings (Petters and Kreidenweis, 2007; Rudich et al., 2007). Such interactions may arise from the transport of aerosol particles or interactions with sunlight, other particulate matter, or with water (Seinfeld and Pandis, 2006; Wong et al., 2011).

Among the individual types of aerosol particles previously investigated, mineral dust is of particular importance because of its high abundance in the atmosphere (Ganor and Mamane, 1982; Ganor and Foner, 1996; Chou et al., 2008; Coz et al., 2009) and its demonstrated ability to nucleate cloud droplets (Herich et al., 2009; Koehler et al., 2009; Sullivan et al., 2009; Kumar et al., 2011a, b). It is also important for primary production in oceans and rain forests because air masses laden with crustal material often transport limiting nutrients like iron and phosphorus (Duce et al., 1991; Pett-Ridge, 2009). Mineral dust is lofted into the atmosphere when wind blows over arid soil, via a process known as saltation, and over half of wind-blown atmospheric aerosol origi-

ACPD
13, 31041–31078, 2013

nates from such sources (Tegen et al., 1996). Though mineral dust in the atmosphere mainly arises from naturally arid regions, it can also be mobilized anthropogenically, via land-use change, and is an additional aspect of the climate system changing over time (Forster and Ramaswamy, 2007). Recent satellite observations estimate that 25 % of mineral dust comes from anthropogenic sources (Ginoux et al., 2012).

The behavior of mineral dust as a CCN depends on its physical and chemical properties. This study investigates the activation potential of three common clay minerals – illite, sodium-rich montmorillonite (NaMon), and Arizona Test Dust (ATD) – and compares the findings with those in the literature. The particular mineral dust samples considered in this study are commonly observed in the atmosphere (Usher et al., 2003) and have been studied previously. The empirical results from both this and previous works are interpreted with respect to the theoretical descriptions of warm cloud droplet activation, κ-Köhler theory and FHH theory. This study considers the effect of generation method on activation potential using electron microscopy (EM), ion chromatography (IC) and Particle Analysis by Laser Mass Spectrometry (PALMS), comparing the results for dry- and wet-generated aerosol. Though many studies in the literature, e.g. Herich et al. (2009) and Koehler et al. (2009), have used the method of atomizing mineral dust particles from a wet slurry, more recent work (Sullivan et al., 2009; Kumar et al., 2011b) has indicated that wet atomization of mineral dust particles leads to anomalous results in their activation. The effects of these artifacts are quantified, and their impacts on experimental results are considered.

2 Theoretical framework

2.1 κ-Köhler theory

Köhler theory provides a theoretical basis for describing the equilibrium vapor pressure of a liquid droplet as it relates to the droplet's diameter (Köhler, 1936). It considers both the effects on saturation vapor pressure due a curved surface (the Kelvin effect) and

ACPD
13, 31041–31078, 2013

the presence of a solute (Raoult's Law) (Köhler, 1936). Subsequently, this theory was adapted to account for differing solute hygroscopicity and to allow for easier parameterization in models (Junge and McLaren, 1971; Fitzgerald, 1973). A recent approach to describe the relationship between a particle's dry diameter, D_d, and its activity as a CCN relates these two quantities by parameterizing a particle's hygroscopicity with a single parameter, κ (Petters and Kreidenweis, 2007). Derivation of κ-Köhler theory starts with the Kelvin relation for the saturation ratio over a curved surface:

$$S = a_w \exp\left(\frac{4\sigma M_w}{RT\rho_w D}\right) \quad (1)$$

where a_w is the activity of water in solution, ρ_w is the density of water, M_w is the molecular weight of water, σ is the surface tension of the edge of the droplet, R is the universal gas constant, T is temperature, and D is the diameter of the droplet. In the κ-Köhler parameterization, the hygroscopicity parameter κ is defined via the dependence of the activity of water in a solution on the solute hygroscopicity:

$$\frac{1}{a_w} = 1 + \kappa\frac{V_s}{V_w} \quad (2)$$

where V_s is the volume of the dry particulate matter and V_w is the volume of the water. The volumes in Eq. (2) can be expressed as equivalent diameters, since $D_i^3 = 6V_i/\pi$. Solving Eq. (2) for a_w and substituting the result into Eq. (1), provides a relation for S in terms of D_d (the dry particle diameter), κ, S, and D:

$$S(D) = \frac{D^3 - D_d^3}{D^3 - D_d^3(1-\kappa)} \exp\left(\frac{4\sigma M_w}{RT\rho_w D}\right) \quad (3)$$

Determined experimentally, values for κ lie between 0.5 and 1.4 for the most hygroscopic CCN, such as salts; between 0.01 and 0.5 for moderately hygroscopic species;

ACPD
13, 31041–31078, 2013

and approach zero for hydrophobic species (Petters and Kreidenweis, 2007). Observational studies have shown that typical atmospheric aerosols have κ between 0.1 and 0.9 (Petters and Kreidenweis, 2007). For the materials considered in this study, the literature suggests that $\kappa = 0.03$ for ATD, illite, and NaMon (Herich et al., 2009).

2.2 FHH adsorption activation theory

Studies of cloud nucleation on insoluble particles have suggested that condensation on such particles may occur via multilayer adsorption (McDonald, 1964). FHH adsorption activation theory has recently been suggested as a framework to describe CCN activity because it includes the effects of water adsorption on the insoluble component of the dust particles. It, like κ-Köhler theory, starts with the Kelvin relation (Eq. 1). However, the FHH framework is more complex and includes an adsorption term in the Kelvin relation instead of the solute term, because it asserts that including adsorption in a CCN activity model more accurately estimates the equilibrium growth of insoluble particles and better determines their critical supersaturation. To describe the formulation of FHH theory, a_w in Eq. (1) is replaced with an FHH isotherm, $a_w = \exp(-A/\Theta^{-B})$, where Θ is the Brunauer, Emmet and Teller (BET) isotherm:

$$\Theta = \frac{cS}{(1-S)(1-S-cS)} \tag{4}$$

and A and B are parameters found using a least squares fit to empirical data. In Eq. (4), c is a constant related to the heat of adsorption and S is the saturation ratio of the gas. This formulation provides the expression for the equilibrium saturation ratio for a solution droplet according to FHH theory:

$$S = \exp(-A/\Theta^{-B}) \exp\left(\frac{4\sigma M_w}{RT\rho_w D}\right) \tag{5}$$

ACPD
13, 31041–31078, 2013

3 Methodology

3.1 Samples

The dust types investigated are "Nominal 0–3 µm" ATD from Powder Technology Inc., illite (rock chips from Clay Mineral Society), and NaMon (unspecified size powder from Clay Mineral Society). In order to increase the number of particles in the desired size range (100–1000 nm, in all cases diameter) all samples are ground in a Fisher Model 8-323V2 Mortar Grinder, using agate pestle and mortar, for 3 h in ethanol. This wet-grinding process is known to result in thinner crystalline sheets and is less likely to degrade clay crystallinity than dry-grinding (Cicel and Kranz, 1981). Though grinding is required to generate particles of the desired sizes, it should be noted that this grinding technique might not reproduce natural weathering processes and could lead to particle properties, such as surface roughness, that are different from those observed in nature.

To assess the effect that grinding has on the activation behavior of the resulting powder CCN activation was compared between ground and unground ATD. The size-dependent critical activation of the ground and unground ATD are identical within measurement uncertainty (Table 1), affirming that the grinding process does not change the activation behavior. IC experiments indicating similar soluble material concentrations in ground and unground samples are detailed in a later section.

3.2 Experimental setup

The setup for CCN activation experiments (shown in Fig. 1) consists of four parts: (1) aerosol generation, (2) aerosol size selection, (3) particle counting, and (4) CCN counting. A complementary series of observations are made with EM, IC, and single particle mass spectrometry: EM is used for observing particle morphology, and the latter two are used for investigating the composition and abundance of soluble species in the samples.

ACPD
13, 31041–31078, 2013

3.2.1 Particle generation

Dry-generation of aerosols is accomplished via saltation. ~4.5 g of mineral dust are placed in an Erlenmeyer flask that also contains three 1 cm Teflon-coated stir bars. This flask is shaken by a Lab Line 3589 Shaker to agitate the dust, and flowing air is introduced to suspend particles. The inlet of the flask is fitted with a filter to ensure particle-free air entering the system. This method generates polydisperse aerosol particles with a size distribution that resembles naturally saltated dust (Lafon et al., 2006). Next, the flow is routed through an unshaken Erlenmeyer flask, used as a buffer volume in order to maintain a constant particle concentration and size distributions during an experiment. In order to assess the potential contribution of larger particles, this setup is compared to one that feeds the saltated dust into two URG Corporation cyclone impactors whose 50 % cut sizes are 2.5 µm and 1.0 µm at 16.7 L min^{-1} flow (red arrows in Fig. 1). 2 L min^{-1} of dry nitrogen is used to agitate the dust and 14.7 L min^{-1} dry nitrogen is added to form the remainder of the flow. Any excess flow that is not drawn into the differential mobility analyzer (DMA) is vented into a fume hood using a T-connector (Fig. 1).

To wet-generate particles a Brechtel Manufacturing, Inc. (BMI) 9203 Aerosol Generator is used, which atomizes particles from a solution or slurry. In this study, slurries are created from 1.0 grams of sample mixed with 250 mL double distilled de-ionized 18.2 MΩ Millipore (DDI) water. The droplet-laden air stream enters an in-line dryer that desiccates the droplets such that only their dry nuclei exit the device. Since the flow out of the atomizer is 2 L min^{-1}, a T-connector and filter are placed at its outlet to allow for the excess flow to escape.

3.2.2 Particle sizing and counting

The polydisperse flow (from either the dry or wet generation) is fed into a BMI 2002 DMA, which is fitted with an impactor that has a 50 % cutoff at 650 nm for 1 L min^{-1} of flow. Next, the flow passes through the neutralizer region of the DMA, where the

ACPD
13, 31041–31078, 2013

polydisperse flow is imparted with a known (approximately Boltzmann) charge distribution using strips of Polonium-210. The particles are then sized based on their electrical mobility:

$$Z_p = \frac{neC_c}{3\pi\mu D_{me}} \quad (6)$$

where n is the number of elementary electrical charges carried by the particle, e is the charge of an electron, C_c is the Cunningham slip correction factor, μ is the dynamic viscosity of air, and D_{me} is the mobility equivalent diameter (BMI, 2012). The output flow is pseudo-monodisperse, in that it also contains multiply charged particles with mobility equivalent diameters that are integer multiples of the desired diameter (Hurd and Mullins, 1962). Next, the particles pass through a flow splitter, where a portion (0.36 L min^{-1}) of the monodisperse flow is routed to a BMI 1700 Mixing Condensation Particle Counter (MCPC) that records the total generated number concentration, N_T, at 1 Hz frequency. Over the course of an experiment, the setup allows either for scans across a 10–1000 nm size range (i.e., SMPS scans) or to set Z_p to a desired value. The DMA sheath flow is set to 5 L min^{-1} to maintain a fixed ratio with the sample flow rate.

3.2.3 CCN counting

The remaining 1 L min^{-1} of monodisperse flow from the DMA is fed into a subsequent flow splitter whose terminals feed into the two chambers in a Droplet Measurement Technologies Model CCN-200 Cloud Condensation Nuclei Counter (CCNC) (Roberts and Nenes, 2005; Lance et al., 2006). The CCNC measures the number concentration of particles that have condensed droplets, N_a, via internal Optical Particle Counters (OPC's) (Roberts and Nenes, 2005). Each of the two chambers in the CCNC draws 0.5 L min^{-1}. The sum of these flow rates plus that drawn by the MCPC yields the total sample flow rate of 1.36 L min^{-1} through the system.

ACPD
13, 31041–31078, 2013

The two columns in the CCNC can be set to a range of supersaturations, S. For the purpose of this study, chamber A scans over S = 0.07, 0.1, 0.3, and 0.05, while chamber B scans over S = 0.7, 0.5, 0.3, and 0.71. The first three supersaturations (for both chambers) have a six-minute duration. The final supersaturation in each chamber (0.05 and 0.71, respectively) lasts for two minutes and is included for equilibrating the CCNC before starting the next scan. The S values for this last step are selected to be outside the typical operational range of the CCNC so they can be removed as adjustment periods in the data. Running a sample at a specific size requires 18 min, with an additional two minutes to equilibrate the column temperatures and switch to the next size with the DMA. In a single scan, the fraction of activated CCN is reported at supersaturations of S = 0.07, 0.1, 0.3, 0.5, and 0.7. The supersaturation at which 50 % of the particles activate into droplets is called the critical supersaturation, S_{crit}, which is found by fitting a sigmoid curve to the N_a/N_T vs. S data. Since both chambers simultaneously collect data for S = 0.3, a comparison is made to verify S and N_a is comparable between the chambers.

3.2.4 Ion chromatography

Examination of the soluble components of the mineral dust is accomplished using IC. Samples are prepared by mixing 0.5 g of each of the ground and unground powders with 50 mL of DDI water, and filtering the resulting supernatant successively though 0.45 µm, 0.2 µm, and 0.02 µm, sterile syringe filters to produce a solution of the soluble species in the sample. Anions and cations are analyzed using a Dionex DX-500 ion chromatograph equipped with electrochemical suppression and a conductivity detector. For anions a Dionex AS15 analytical column is used with a sodium hydroxide eluent. For cations a CS12A analytical column is used with a sulfuric acid eluent. The measurable cations are sodium, lithium, potassium, calcium, magnesium, strontium, and ammonium. The measurable anions are chloride, bromide, nitrate, sulfate, and fluorine. This list accounts for the most likely ions to be leached from clay minerals (Wenk and Bulakh, 2004).

ACPD
13, 31041–31078, 2013

3.2.5 Electron microscopy

Transmission EM is used to investigate the morphological properties of the aerosol particles considered in this study. In order to analyze samples, they are generated and size-selected as described above and then are collected using a conventional impactor, similar to the MOUDI M135-10 impactor. Particles are impacted onto Electron Microscopy Sciences FCF200 gold microscope grids with formvar carbon support film. Grid analysis is performed at the MIT Center for Materials Science and Engineering using a JEOL 2010 Advanced High Performance TEM to determine the sizes and aspect ratios of the particles. Additionally, the energy-dispersive X-ray (EDX) spectroscopy functionality of this microscope enables characterization of the samples based on elemental abundance.

3.2.6 Particle analysis by laser mass spectrometry

PALMS (Murphy and Thompson, 1995; Cziczo et al., 2006) is used to investigate the aerodynamic size and chemical composition of monodisperse dust particles. The chemical differences in dry- and wet-generated particles are of particular interest. Spectra are collected on a particle-by-particle basis and 1000 spectra are gathered per sample per size. Aerosol particles enter PALMS via an aerodynamic inlet. A Nd:YAG laser beam is split into two beams to detect the particle, using the time between scattering events to provide aerodynamic size information. Next, a 193 nm excimer laser is triggered to ablate and ionize the particle. The ions from the particle are sent through a reflectron and registered on a micro-channel plate to record a mass spectrum for the particle. Both positive and negative mass spectra are recorded for the dust samples.

ACPD
13, 31041–31078, 2013

3.3 Data processing

3.3.1 Charge correction

Particles passing through the charge neutralizer in the DMA are imparted with an equilibrium charge distribution that can be approximated by a Boltzmann distribution (BMI, 2012). The fraction of particles with a particular charge can be calculated using the method of Wiedensohler et al. (1988). With this technique, measuring the incoming polydisperse size distribution allows for the determination of the number of multiply charged particles in the monodisperse output.

When determining the incoming polydisperse size distribution into the DMA, charge corrections are applied that reassign multiply charged particles to the correct size bins, assuming that a known fraction of each bin is multiply charged (BMI, 2012). This procedure produces a charge-corrected critical supersaturation, $S_{\mathrm{crit,cc}}$. This method is appropriate for size distributions that are smooth but creates an artifact for distributions that do not span the entire range of a scan, which is the case for dry-generated mineral dust. As seen in Fig. 2, sampling from the apparent tail of such a distribution yields only multiply charged particles, leading to a significant data artifact. As shown in a later section, this lack of correctly sized particles is supported by EM results: for mobility equivalent sizes smaller than $\sim$ 300 nm, EM shows only multiply charged particles whose diameters are integer multiples of the desired size.

3.3.2 Shape correction

A particle's mobility equivalent diameter, D_{me}, is defined as the diameter of a sphere with the same electrical mobility as the particle. Therefore, the D_{me} of a particle corresponds to its actual diameter if the particle is spherical (DeCarlo et al., 2004). For a non-spherical particle the electrical mobility is insufficient to determine the surface area that is available for interactions with water (DeCarlo et al., 2004; Kumar et al., 2011a). The volume equivalent diameter, D_{ve}, of a particle is defined as the diameter

ACPD
13, 31041–31078, 2013

of a sphere with the same volume as an irregularly shaped particle. The relationship between D_{me} and D_{ve} is typically analyzed using tandem electrical mobility and aerodynamic particle sizing to determine the dynamic shape factor, χ, of the irregularly shaped particle (DeCarlo et al., 2004; Kumar et al., 2011a). χ is defined as the ratio of drag force experienced by the irregularly-shaped particle to that experienced by a sphere with equivalent volume as both move through a gas at the same velocity (DeCarlo et al., 2004). A spherical particle has $\chi = 1$, and $D_{me} = \chi D_{ve}$, with $\chi \geq 1$. Since $D_{me} \geq D_{ve}$, knowing a particle's mobility equivalent diameter provides an upper bound for the volume of a non-spherical particle.

The clay minerals considered in this study are non-spherical. They have a layered chemical structure and a flat or sheet-like morphology (Wenk and Bulakh, 2004). Mineral dust particles are approximated as elliptical cylinders with major axis, d_M, and minor axis, d_m, and maximum thickness, h_{max}, which is constrained by mobility sizing. The expression for the maximum thickness is:

$$h_{max} = \frac{2D_{me}^3}{3d_M d_m} \quad (7)$$

Electron micrographs provide a means to determine the dimensions of the cylindrical face, and the particle's mobility diameter provides an upper bound on the height by bounding its volume. The micrographs can also indicate whether a particle is being observed edge-on or face-on because a particle's face does not exhibit the stratified structure that an edge does. For each sample, direct EM observations exist for dry-generated particles with $D_{me} = 200$ and 400 nm, and for wet-generated particles of $D_{me} = 50$, 100, and 400 nm. Since wet-generated NaMon has a unimodal size distribution, EM observations at $D_{me} = 50$ and 400 nm are sufficient to investigate its morphology as a function of size.

As a particle's thickness approaches zero its surface area equals twice the face area. Per Kumar et al. (2011a) and Kumar et al. (2011b), the surface area equivalent diameter, D_{se}, is defined as the diameter of a sphere having the same surface area as

ACPD
13, 31041–31078, 2013

an irregularly shaped particle. Assuming particles have a non-zero height and volume less than a sphere of diameter D_{me}, the bounds on D_{se} are:

$$\sqrt{\frac{1}{2}d_M d_m} < D_{se} < \sqrt{\frac{1}{2}d_M d_m + \frac{1}{3}(d_M + d_m)\frac{D_{me}^3}{d_M d_m}} \quad (8)$$

The effects of charge and shape corrections for correctly sized, dry-generated particles are shown in Table 2, and those for dry-generated ATD are seen in Fig. 3. Charge-corrected critical supersaturations are higher than uncorrected ones because the contribution of multiply charged particles is removed. Shape-corrected surface area equivalent diameters tend to be larger than their corresponding mobility diameters because of particle non-sphericity. The effects of charge and shape correction are of similar importance for ATD. The shape corrections for all the samples have similar increases in equivalent diameter, but the effects of charge correction for illite and NaMon are more significant because of their lower uncorrected critical supersaturations.

4 Results

The size-dependent particle concentration for dry-generated (black squares), wet-generated (blue squares), and dry-generated cyclone impacted (red squares) particles were determined using SMPS scans for each dust type and dispersion method (Fig. 4). The dry-generated particles are most prevalent at larger sizes, and the concentration is significantly less for sizes below ~ 300 nm. The wet-generated size distributions are all significantly different from their dry counterparts. The size distribution of the dry-generated cyclone-impacted particles resembles that of the dry-generated particles, but the overall concentration of particles is lower and the peak concentration is shifted to a smaller size. For ATD and illite, the wet distributions are bimodal, and for NaMon the peak of the wet distribution is shifted to a smaller size. As noted above, previous studies have indicated that wet generation methods introduce a significant artifact that

ACPD
13, 31041–31078, 2013

is not found with dry dispersion, i.e. atomized aerosols may contain soluble contaminants or metastable hydrates that are not found in dry-dispersed aerosols (Sullivan et al., 2009; Kumar et al., 2011b). With respect to the size distribution, this artifact corresponds to the peak at ∼ 50 nm that is not present in the dry distributions (Fig. 4).

The wet generation artifact manifests as a mode of soluble non-mineral particles whose influence is observable using IC, EM, and PALMS. Figure 5 shows the results from the IC analysis of the soluble portions of the clay samples, which likely comprises the smaller mode seen in the size distributions. The ground and unground results are similar, and the grinding process does not preferentially increase or decrease the amount of dissolved material. NaMon leaches more sodium but less significant quantities of the other materials than the other clays. This increase is likely observed because NaMon is a swelling clay, where the mineral layers are less tightly bound and therefore hydrate more efficiently (Foster, 1953; Poppe et al., 2001). The smaller mobility diameter peak in the ATD and illite wet-generated size distributions is likely comprised of leeched soluble material. Since water can more easily permeate between layers in NaMon, the unimodal wet-generated size distribution is likely a result of incomplete drying of particles after interaction with water. The sizes of salt particles formed from wet generation can be estimated by summing the concentration of all dissolved material measured by the IC and assuming a typical density for the resulting salts of 2.3 g cc^{-1}. Since the atomizer produces droplets whose mode size is 1.5 µm, the resulting particles are 40–50 nm. This size corresponds to the smaller peak in the bimodal size distributions.

Figure 6 shows the typical EDX peaks for each clay species at several mobility-equivalent sizes from the EDX detector on the JEOL 2010 Advanced High Performance TEM. There is little size dependence of soluble material content in both dry- and wet-generated mineral dusts. Wet-generated particles have more elemental variety than dry-generated particles, further suggesting a redistribution of soluble material to the surface of particles during atomizing. The PALMS spectral data in Fig. 7 further indicates redistribution of soluble material. The figure shows histograms of the area under

ACPD
13, 31041–31078, 2013

cation spectral peaks of 400 nm particles, which correlates with relative abundance of soluble material in these particles. The wet generated particles show a shift toward smaller peak areas, suggesting less relative abundance of soluble material in large wet-generated dust particles.

Shape determination using electron micrographs show that approximating particle geometry as flat and cylindrical is appropriate for the purpose of shape correction (Fig. 4). The images indicate that particles are often larger than their intended mobility size. This is a consequence of the sizing artifact illustrated in Fig. 2. Incorrect sizing occur when attempting to sample from the lower tail of the size distribution where most particles are incorrectly sized. Classifying particles by their mobility-equivalent diameters is only appropriate if the abundance of singlets is much higher than *n*-lets (where *n* is 2 and greater) in the actual size distribution.

Accounting for these multiply charged particles considerably increases the required supersaturation for droplet activation (Fig. 3). Considering non-sphericity to determine surface area also leads to an increase in particle size. Shape corrections are applied only to particles that are sized correctly according to their electrical mobility (squares in Fig. 4). When EM results indicate that the majority of particles are doublets and triplets (stars in Fig. 4), mineral dust of the desired size is not considered present in the sample. In these cases no shape correction is performed since the measurement would not be for particle of the correct size and/or composition.

The above methodology to remove large particles is useful when their abundance in the polydisperse size distribution is large. Using cyclone impaction efficiently removes the larger particles before they enter the DMA and the downstream particle distribution is closer to monodisperse (Fig. 8). The PALMS results indicate that the distributions peak at the desired size and that the majority of doublets and triplets are removed. Therefore, when the influence of larger particles is diminished, standard charge correction procedures (Wiedensohler et al., 1988) can be used to account for the remaining particles. Though EM would be required to determine the exact degree of shape

ACPD
13, 31041–31078, 2013

correction required, these corrections are less important when the larger particles are efficiently removed.

5 Discussion

There is agreement in the charge- and shape-corrected activation results in this study and those found in Kumar et al. (2011a) and Kumar et al. (2011b) (Figs. 4 and 9). The exception is an inability to reproduce the Kumar et al. (2011b) 100 % activation of the larger mode of wet-generated ATD. Illite and NaMon in this study require lower critical supersaturations than those reported in Herich et al. (2009). Since the uncorrected results also do not agree, this disparity may be related to physical or chemical differences in the samples or differences in generation technique. Repeating the CCN activation experiments with cyclone impaction upstream of the DMA yields results that agree with those performed without the impactors if the necessary corrections are made. Impaction greatly reduces the concentration of multiply charged particles, bringing the post-DMA sizes closer to the desired mobility size (Figs. 4 and 8).

Dry-generated particles smaller than $D_{\mathrm{me}} \sim 300$ nm are incorrectly sized because of the high abundance of multiply charged particles. For larger sizes, the critical supersaturations in this study and Kumar et al. (2011a, b) are in agreement. The FHH fits from Kumar et al. (2011a) may be biased by the size artifact observed in this study and no evidence is provided to indicate that the smaller particles were corrected. Since both FHH and κ-Köhler theory agree at the larger sizes, the simpler parameterization in κ-Köhler theory is a more suitable framework to describe clay mineral dust nucleation activity, and the complexity introduced by FHH theory is not required when size is corrected. This result also shows that it is vital to consider the appropriate data corrections to find correct values for κ.

In the case of ATD there is an apparent discontinuity in κ at the smallest sizes considered even when size is corrected. Because ATD is an industrially derived sample that is mechanically ground more than in either nature or in the laboratory, these small

ACPD
13, 31041–31078, 2013

sizes are not valid for the atmosphere and may be subject to unknown artifacts, possibly compositional, which are responsible for the discontinuity. The data are provided here for reference but are omitted when determining κ.

Atomizing mineral dust from a slurry is determined to be an unacceptable generation method to simulate saltation of fresh, unprocessed dust particles. Wet generation redistributes soluble material (Figs. 6 and 7), changing the size distributions and critical activations (Fig. 4). There is less difference between generation methods for NaMon because it is a swelling clay. However, it does not avoid the size-dependent partitioning of soluble material (Fig. 7) despite its tendency to trap water between crystal layers.

6 Conclusions and atmospheric implications

Understanding the nucleation of droplets on atmospheric aerosols is a vital step towards describing their role in the climate system. Laboratory studies facilitate understanding CCN activation potential and provide insight into describing these phenomena theoretically and in climate models. This study investigates the activation potential of three mineral dusts to ascertain the suitability of dry and wet generation methods and to determine whether FHH theory or κ-Köhler theory better predicts their critical supersaturations. κ-Köhler theory is found to be appropriate for describing droplet activation on mineral dust if charge and shape corrections are applied. With charge corrections, the size distributions of dust particles must be considered since abundant multiply charged particles could be misidentified as correctly sized smaller particles.

The results of this study agree with recent work (Sullivan et al., 2009; Kumar et al., 2011b) that finds wet-generation to introduce a soluble mode artifact at the smaller mobility sizes (less than $\sim$ 300 nm diameter) of ATD and illite. No dry-generated mineral particles below this size are observed. The wet generation process produces a mode of soluble material liberated from the mineral. The effective κ of these small soluble particles is a different than the κ of the dust. This change in nucleation behavior using wet-generation is not observed when the dust is simply wetted and re-dried.

ACPD
13, 31041–31078, 2013

For swelling clays, such as NaMon, wet-generation does not change the droplet activation properties but it does change the size distribution. Particles do not dehydrate efficiently, akin to the different deliquescence and efflorescence points of inorganic salts. Although a secondary soluble mode is not formed for swelling clays, the added uptake of water implies that these particles are no longer unprocessed dust.

This study suggests caution in the use of wet-dispersion of mineral dust slurries when a comparison to atmospheric particles is to be made. No known atmospheric processes lead to the redistribution of soluble material among large numbers of particles (100's or more), as is the case in atomization of a slurry. This technique inadequately represents a cloud process where mineral dust activates a droplet and then is subsequently released to the environment when the droplet evaporates, as is the case in virga. This study also suggests the simulation of cloud processed (i.e., previously-wetted) mineral dust in the laboratory would be most correctly performed by activating droplets with a CCNC and then evaporating the condensed phase water downstream. This type of procedure could be useful to simulate the physical or chemical processing of particulate matter in clouds.

For representation in aerosol models, the results from this study indicate that it is reasonable to assign mineral dust a κ value of 0.01–0.1. The single exception observed was < 200 nm diameter ATD. However, to produce this size, mechanical grinding for several hours is necessary and is unlikely to be representative of a natural process.

Acknowledgements. We acknowledge NOAA OAR Climate Program Office, award number NA11OAR4310159, for funding and the MIT Center for Materials Science and Engineering for access to the EM facilities. We thank Rachel Keeler for assistance with the EM analyses and the MIT Igneous Petrology Laboratory for assistance with sample preparation.

ACPD
13, 31041–31078, 2013

References

Abbatt, J. P. D., Broekhuizen, K., and Kumal, P. P.: Cloud condensation nucleus activity of internally mixed ammonium sulfate/organic acid aerosol particles, Atmos. Environ., 39, 4767–4778, doi:10.1016/j.atmosenv.2005.04.029, 2005.

Albrecht, B. A.: Aerosols, cloud microphysics, and fractional cloudiness, Science, 245, 1227–1230, doi:10.1126/science.245.4923.1227, 1989.

Bergstrom, R. W., Schmidt, K. S., Coddington, O., Pilewskie, P., Guan, H., Livingston, J. M., Redemann, J., and Russell, P. B.: Aerosol spectral absorption in the Mexico City area: results from airborne measurements during MILAGRO/INTEX B, Atmos. Chem. Phys., 10, 6333–6343, doi:10.5194/acp-10-6333-2010, 2010.

Bilde, M. and Svenningsson, B.: CCN activation of slightly soluble organics: the importance of small amounts of inorganic salt and particle phase, Tellus B, 56, 128–134, doi:10.1111/j.1600-0889.2004.00090.x, 2004.

BMI: Brechtel Manufacturing Incorporated Model 2002 Scanning Electrical Mobility System Manual, 5.5 ed., Hayward, CA, 2012.

Booth, B. B. B., Dunstone, N. J., Halloran, P. R., Andrews, T., and Bellouin, N.: Aerosols implicated as a prime driver of twentieth century North Atlantic climate variability, Nature, 484, 228–232, doi:10.1038/nature10946, 2012.

Brock, C. A., Cozic, J., Bahreini, R., Froyd, K. D., Middlebrook, A. M., McComiskey, A., Brioude, J., Cooper, O. R., Stohl, A., Aikin, K. C., de Gouw, J. A., Fahey, D. W., Ferrare, R. A., Gao, R.-S., Gore, W., Holloway, J. S., Hübler, G., Jefferson, A., Lack, D. A., Lance, S., Moore, R. H., Murphy, D. M., Nenes, A., Novelli, P. C., Nowak, J. B., Ogren, J. A., Peischl, J., Pierce, R. B., Pilewskie, P., Quinn, P. K., Ryerson, T. B., Schmidt, K. S., Schwarz, J. P., Sodemann, H., Spackman, J. R., Stark, H., Thomson, D. S., Thornberry, T., Veres, P., Watts, L. A., Warneke, C., and Wollny, A. G.: Characteristics, sources, and transport of aerosols measured in spring 2008 during the aerosol, radiation, and cloud processes affecting Arctic Climate (ARCPAC) Project, Atmos. Chem. Phys., 11, 2423–2453, doi:10.5194/acp-11-2423-2011, 2011.

Chou, C., Formenti, P., Maille, M., Ausset, P., Helas, G., Harrison, M., and Osborne, S.: Size distribution, shape, and composition of mineral dust aerosols collected during the African Monsoon Multidisciplinary Analysis Special Observation Period 0: dust and biomass-burning

ACPD
13, 31041–31078, 2013

experiment field campaign in Niger, January 2006, J. Geophys. Res.-Atmos, 113, D00C10, doi:10.1029/2008jd009897, 2008.
Christopher, S. A., Johnson, B., Jones, T. A., and Haywood, J.: Vertical and spatial distribution of dust from aircraft and satellite measurements during the GERBILS field campaign, Geophys. Res. Lett., 36, L06806, doi:10.1029/2008GL037033, 2009.
Cicel, B. and Kranz, G.: Mechanism of montmorillonite structure degradation by percussive grinding, Clay Min., 16, 151–162, doi:10.1180/claymin.1981.016.2.03, 1981.
Coz, E., Gomez-Moreno, F. J., Pujadas, M., Casuccio, G. S., Lersch, T. L., and Artinano, B.: Individual particle characteristics of North African dust under different long-range transport scenarios, Atmos. Environ., 43, 1850–1863, doi:10.1016/j.atmosenv.2008.12.045, 2009.
DeCarlo, P. F., Slowik, J. G., Worsnop, D. R., Davidovits, P., and Jimenez, J. L.: Particle morphology and density characterization by combined mobility and aerodynamic diameter measurements. Part 1: Theory, Aerosol Sci. Tech., 38, 1185–1205, doi:10.1080/027868290903907, 2004.
Denman, K. L., Brasseur, G., Chidthaisong, A., Ciais, P., Cox, P. M., Dickinson, R. E., Hauglustaine, D., Heinze, C., Holland, E., Jacob, D., Lohmann, U., Ramachandran, S., da Silva Dias, P. L., Wofsy, S. C., and Zhang, X.: Couplings between changes in the climate system and biogeochemistry, in: Climate Change 2007: The Physical Science Basis, Contribution of Working Group I to the Fourth Assessment Report of the Intergovernmental Panel on Climate Change, edited by: Solomon, S., Qin, D., Manning, M., Chen, Z., Marquis, M., Averyt, K. B., Tignor, M., and Miller, H. L., Cambridge University Press, Cambridge, UK and New York, NY, USA, 499–587, 2007.
Duce, R. A., Liss, P. S., Merrill, J. T., Atlas, E. L., Buat-Menard, P., Hicks, B. B., Miller, J. M., Prospero, J. M., Arimoto, R., Church, T. M., Ellis, W., Galloway, J. N., Hansen, L., Jickells, T. D., Knap, A. H., Reinhardt, K. H., Schneider, B., Soudine, A., Tokos, J. J., Tsunogai, S., Wollast, R., and Zhou, M.: The atmospheric input of trace species to the world ocean, Global Biogeochem. Cy., 5, 193–259, doi:10.1029/91GB01778, 1991.
Dusek, U., Frank, G. P., Hildebrandt, L., Curtius, J., Schneider, J., Walter, S., Chand, D., Drewnick, F., Hings, S., Jung, D., Borrmann, S., and Andreae, M. O.: Size matters more than chemistry for cloud-nucleating ability of aerosol particles, Science, 312, 1375–1378, doi:10.1126/science.1125261, 2006.

ACPD
13, 31041–31078, 2013

Fitzgerald, J. W.: Dependence of supersaturation spectrum of CCN on aerosol size distribution and composition, J. Atmos. Sci., 30, 628–634, doi:10.1175/1520-0469(1973)030<0628:dotsso>2.0.co;2, 1973.
Forster, P., Ramaswamy, V., Artaxo, P., Berntsen, T., Betts, R., Fahey, D. W., Haywood, J., Lean, J., Lowe, D. C., Myhre, G., Nganga, J., Prinn, R., Raga, G., Schulz, M., and Van Dorland, R.: Changes in atmospheric constituents and in radiative forcing, in: Climate Change 2007: The Physical Science Basis, Contribution of Working Group I to the Fourth Assessment Report of the Intergovernmental Panel on Climate Change, edited by: Solomon, S., Qin, D., Manning, M., Chen, Z., Marquis, M., Averyt, K. B., Tignor, M., and Miller, H. L., Cambridge University Press, Cambridge, UK and New York, NY, USA, 129–234, 2007.
Foster, M. D.: Geochemical studies of clay minerals, 2. Relation between ionic substitution and swelling in montmorillonites, Am. Mineral., 38, 994–1006, 1953.
Ganor, E. and Foner, H. A.: The mineralogical and chemical properties and the behaviour of Aeolian Saharan dust over Israel, Envir. Sci. Tech. Lib., 11, 163–172, 1996.
Ganor, E. and Mamane, Y.: Transport of Saharan dust across the eastern Mediterranean, Atmos. Environ., 16, 581–587, doi:10.1016/0004-6981(82)90167-6, 1982.
Ginoux, P., Prospero, J. M., Gill, T. E., Hsu, N. C., and Zhao, M.: Global-scale attribution of anthropogenic and natural dust sources and their emission rates based on MODIS Deep Blue aerosol products, Rev. Geophys., 50, RG3005, doi:10.1029/2012rg000388, 2012.
Hansen, J., Sato, M., Kharecha, P., and von Schuckmann, K.: Earth's energy imbalance and implications, Atmos. Chem. Phys., 11, 13421–13449, doi:10.5194/acp-11-13421-2011, 2011.
Herich, H., Tritscher, T., Wiacek, A., Gysel, M., Weingartner, E., Lohmann, U., Baltensperger, U., and Cziczo, D. J.: Water uptake of clay and desert dust aerosol particles at sub- and supersaturated water vapor conditions, Phys. Chem. Chem. Phys., 11, 7804–7809, doi:10.1039/b901585j, 2009.
Hurd, F. K. and Mullins, J. C.: Aerosol size distribution from ion mobility, J. Coll. Sci. Imp. U. Tok., 17, 91–100, doi:10.1016/0095-8522(62)90001-6, 1962.
Junge, C. and McLaren, E.: Relationship of cloud nuclei spectra to aerosol size distribution and composition, J. Atmos. Sci., 28, 382–390, doi:10.1175/1520-0469(1971)028<0382:rocnst>2.0.co;2, 1971.
Koehler, K. A., Kreidenweis, S. M., DeMott, P. J., Petters, M. D., Prenni, A. J., and Carrico, C. M.: Hygroscopicity and cloud droplet activation of mineral dust aerosol, Geophys. Res. Lett., 36, L08805, doi:10.1029/2009gl037348, 2009.

ACPD
13, 31041–31078, 2013

Kohler, H.: The nucleus in and the growth of hygroscopic droplets, Trans. Faraday Soc., 32, 1152–1161, doi:10.1039/tf9363201152, 1936.

Kumar, P., Sokolik, I. N., and Nenes, A.: Measurements of cloud condensation nuclei activity and droplet activation kinetics of fresh unprocessed regional dust samples and minerals, Atmos. Chem. Phys., 11, 3527–3541, doi:10.5194/acp-11-3527-2011, 2011a.

Kumar, P., Sokolik, I. N., and Nenes, A.: Cloud condensation nuclei activity and droplet activation kinetics of wet processed regional dust samples and minerals, Atmos. Chem. Phys., 11, 8661–8676, doi:10.5194/acp-11-8661-2011, 2011b.

Lafon, S., Sokolik, I. N., Rajot, J. L., Caquineau, S., and Gaudichet, A.: Characterization of iron oxides in mineral dust aerosols: implications for light absorption, J. Geophys. Res.-Atmos, 111, D21207, doi:10.1029/2005jd007016, 2006.

Lambe, A. T., Onasch, T. B., Massoli, P., Croasdale, D. R., Wright, J. P., Ahern, A. T., Williams, L. R., Worsnop, D. R., Brune, W. H., and Davidovits, P.: Laboratory studies of the chemical composition and cloud condensation nuclei (CCN) activity of secondary organic aerosol (SOA) and oxidized primary organic aerosol (OPOA), Atmos. Chem. Phys., 11, 8913–8928, doi:10.5194/acp-11-8913-2011, 2011.

Lance, S., Medina, J., Smith, J. N., and Nenes, A.: Mapping the operation of the DMT Continuous Flow CCN counter, Aerosol Sci. Tech., 40, 242–254, doi:10.1080/02786820500543290, 2006.

Logan, T., Xi, B., Dong, X., Obrecht, R., Li, Z., and Cribb, M.: A study of Asian dust plumes using satellite, surface, and aircraft measurements during the INTEX-B field experiment, J. Geophys. Res., 115, D00K25, doi:10.1029/2010JD014134, 2010.

Lyapustin, A., Gatebe, C. K., Kahn, R., Brandt, R., Redemann, J., Russell, P., King, M. D., Pedersen, C. A., Gerland, S., Poudyal, R., Marshak, A., Wang, Y., Schaaf, C., Hall, D., and Kokhanovsky, A.: Analysis of snow bidirectional reflectance from ARCTAS Spring-2008 Campaign, Atmos. Chem. Phys., 10, 4359–4375, doi:10.5194/acp-10-4359-2010, 2010.

McDonald, J. E.: Cloud nucleation on insoluble particles, J. Atmos. Sci., 21, 109–116, doi:10.1175/1520-0469(1964)021<0109:cnoip>2.0.co;2, 1964.

McFarquhar, G. M., Ghan, S., Verlinde, J., Korolev, A., Strapp, J. W., Schmid, B., Tomlinson, J. M., Wolde, M., Brooks, S. D., Cziczo, D., Dubey, M. K., Fan, J., Flynn, C., Gultepe, I., Hubbe, J., Gilles, M. K., Laskin, A., Lawson, P., Leaitch, W. R., Liu, P., Liu, X., Lubin, D., Mazzoleni, C., Macdonald, A.-M., Moffet, R. C., Morrison, H., Ovchinnikov, M., Shupe, M. D.,

ACPD
13, 31041–31078, 2013

Turner, D. D., Xie, S., Zelenyuk, A., Bae, K., Freer, M., and Glen, A.: Indirect and semi-direct aerosol campaign, B. Am. Meteorol. Soc., 92, 183–201, 2011.
Middlebrook, A. M., Thomson, D. S., and Murphy, D. M.: On the purity of laboratory generated sulfuric acid droplets and ambient particles studied by laser mass spectrometry, Aerosol Sci. Tech., 27, 293–307, 1997.
Murphy, D. M. and Thomson, D. S.: Laser ionization mass spectroscopy of single aerosol particles, Aerosol Sci. Tech., 22, 237–249, doi:10.1080/02786829408959743, 1995.
Noble, C. A. and Prather, K. A.: Real-time measurement of correlated size and composition profiles of individual atmospheric aerosol particles, Environ. Sci. Tech., 30, 2667–2680, doi:10.1021/es950669j, 1996.
Pett-Ridge, J. C.: Contributions of dust to phosphorus cycling in tropical forests of the Luquillo Mountains, Puerto Rico, Biogeochemistry, 94, 63–80, doi:10.1007/s10533-009-9308-x, 2009.
Petters, M. D. and Kreidenweis, S. M.: A single parameter representation of hygroscopic growth and cloud condensation nucleus activity, Atmos. Chem. Phys., 7, 1961–1971, doi:10.5194/acp-7-1961-2007, 2007.
Poppe, L. J., Coastal and Marine Geology Program (Geological Survey), and Geological Survey (US): A laboratory manual for x-ray powder diffraction, in: US Geological Survey open-file report 01-41, US Geological Survey, Coastal and Marine Geology Program, Woods Hole, Mass., 2001.
Pruppacher, H. R. and Klett, J. D.: Microphysics of Clouds and Precipitation, 2nd edn., Atmospheric and Oceanographic Sciences Library, 18, Kluwer Academic Publishers, Dordrecht, Boston, MA, 954, 1997.
Raymond, T. M. and Pandis, S. N.: Cloud activation of single-component organic aerosol particles, J. Geophys. Res.-Atmos, 107, 4787, doi:10.1029/2002jd002159, 2002.
Raymond, T. M. and Pandis, S. N.: Formation of cloud droplets by multicomponent organic particles, J. Geophys. Res.-Atmos, 108, 4469, doi:10.1029/2003jd003503, 2003.
Roberts, G. C. and Nenes, A.: A continuous-flow streamwise thermal-gradient CCN chamber for atmospheric measurements, Aerosol Sci. Tech., 39, 206–221, doi:10.1080/027868290913988, 2005.
Rudich, Y., Donahue, N. M., and Mentel, T. F.: Aging of organic aerosol: bridging the gap between laboratory and field studies, Annu. Rev. Phys. Chem., 58, 321–352, 2007.

ACPD
13, 31041–31078, 2013

Seinfeld, J. H. and Pandis, S. N.: Atmospheric Chemistry and Physics: From Air Pollution to Climate Change, 2nd edn., Wiley, Hoboken, NJ, 1203, 2006.
Shaw, R. W. and Paur, R. J.: Composition of aerosol-particles collected at rural sites in the Ohio River Valley, Atmos. Environ., 17, 2031–2044, doi:10.1016/0004-6981(83)90360-8, 1983.
Sullivan, R. C., Moore, M. J. K., Petters, M. D., Kreidenweis, S. M., Roberts, G. C., and Prather, K. A.: Effect of chemical mixing state on the hygroscopicity and cloud nucleation properties of calcium mineral dust particles, Atmos. Chem. Phys., 9, 3303–3316, doi:10.5194/acp-9-3303-2009, 2009.
Tegen, I., Lacis, A. A., and Fung, I.: The influence on climate forcing of mineral aerosols from disturbed soils, Nature, 380, 419–422, doi:10.1038/380419a0, 1996.
Twomey, S.: Influence of pollution on shortwave albedo of clouds, J. Atmos. Sci., 34, 1149–1152, doi:10.1175/1520-0469(1977)034<1149:tiopot>2.0.co;2, 1977.
Usher, C. R., Michel, A. E., and Grassian, V. H.: Reactions on mineral dust, Chem. Rev., 103, 4883–4939, doi:10.1021/cr020657y, 2003.
Wenk, H.-R. and Bulakh, A. G.: Minerals: their Constitution and Origin, Cambridge University Press, Cambridge, New York, xxii, 646, 2004.
Wiedensohler, A.: An approximation of the bipolar charge-distribution for particles in the submicron size range, J. Aerosol. Sci., 19, 387–389, doi:10.1016/0021-8502(88)90278-9, 1988.
Wong, J. P. S., Lee, A. K. Y., Slowik, J. G., Cziczo, D. J., Leaitch, W. R., Macdonald, A., and Abbatt, J. P. D.: Oxidation of ambient biogenic secondary organic aerosol by hydroxyl radicals: effects on cloud condensation nuclei activity, Geophys. Res. Lett., 38, L22805, doi:10.1029/2011gl049351, 2011.
Yu, H., Kaufman, Y. J., Chin, M., Feingold, G., Remer, L. A., Anderson, T. L., Balkanski, Y., Bellouin, N., Boucher, O., Christopher, S., DeCola, P., Kahn, R., Koch, D., Loeb, N., Reddy, M. S., Schulz, M., Takemura, T., and Zhou, M.: A review of measurement-based assessments of the aerosol direct radiative effect and forcing, Atmos. Chem. Phys., 6, 613–666, doi:10.5194/acp-6-613-2006, 2006.
Zhang, X. Y., Wang, Y. Q., Niu, T., Zhang, X. C., Gong, S. L., Zhang, Y. M., and Sun, J. Y.: Atmospheric aerosol compositions in China: spatial/temporal variability, chemical signature, regional haze distribution and comparisons with global aerosols, Atmos. Chem. Phys., 12, 779–799, doi:10.5194/acp-12-779-2012, 2012.

ACPD
13, 31041–31078, 2013

Table 1. Comparison of uncorrected critical supersaturations for ground and unground ATD.

	100 nm	200 nm	300 nm	400 nm
Ground	0.62 ± 0.04	0.26 ± 0.02	0.24 ± 0.02	0.19 ± 0.02
Unground	0.59 ± 0.01	0.24 ± 0.02	0.21 ± 0.01	0.18 ± 0.02

ACPD
13, 31041–31078, 2013

Table 2. Charge and shape corrections to critical supersaturations of dry particles.

	Uncorrected S_{crit}	Charge Corrected $S_{crit,cc}/S_{crit}$	Shape Corrected D_{se}/D_{me}	Charge and Shape Corrected $D_{se}, S_{crit,cc}$
ATD D_{me} = 300 nm	0.24 ± 0.02	1.33	0.91–1.25	272–374 nm, 0.31 ± 0.04
ATD D_{me} = 400 nm	0.19 ± 0.02	1.22	0.95–1.27	383–508 nm, 0.23 ± 0.02
Illite D_{me} = 300 nm	0.12 ± 0.02	1.54	1.12–1.41	337–422 nm, 0.19 ± 0.04
Illite D_{me} = 400 nm	0.096 ± 0.02	1.80	1.12–1.41	449–563 nm, 0.17 ± 0.05
NaMon D_{me} = 300 nm	0.08 ± 0.03	1.90	1.23–1.51	369–453 nm, 0.15 ± 0.05
NaMon D_{me} = 400 nm	0.06 ± 0.03	1.99	1.23–1.51	492–604 nm, 0.13 ± 0.06

ACPD
13, 31041–31078, 2013

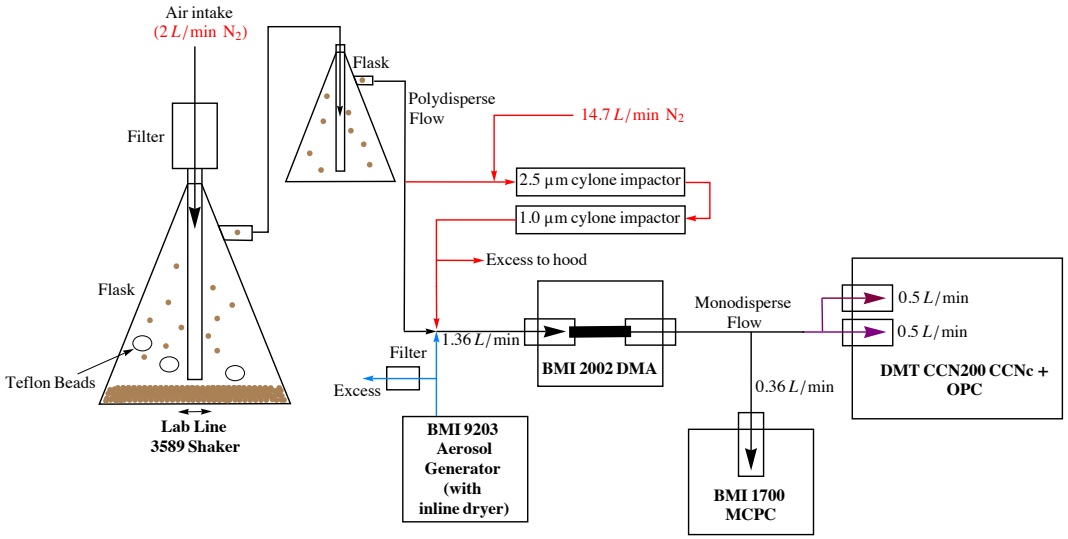

Fig. 1. Diagram of experimental setup with flow rates. Blue arrows indicate the flow path and components used for particle generation from a water-dust slurry (wet-generation). Red arrows indicate the flow paths for using cyclone impaction upstream of the DMA. Purple arrows show the configuration for CCN experiments.

ACPD
13, 31041–31078, 2013

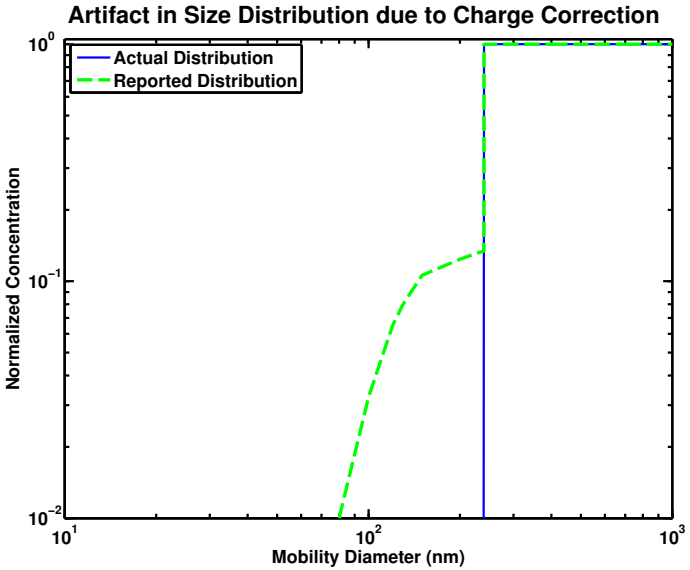

Fig. 2. Artifact introduced into step function size distribution due to SMPS charge corrections. The actual size distribution is shown in blue, and the size distribution reported by a DMA (after charge correction) is shown in dashed green. This difference arises from miss-assigning correctly sized particles to smaller size bins, as would be done for multiply charged particles with the two slopes corresponding to doubly and triply charged particles.

ACPD
13, 31041–31078, 2013

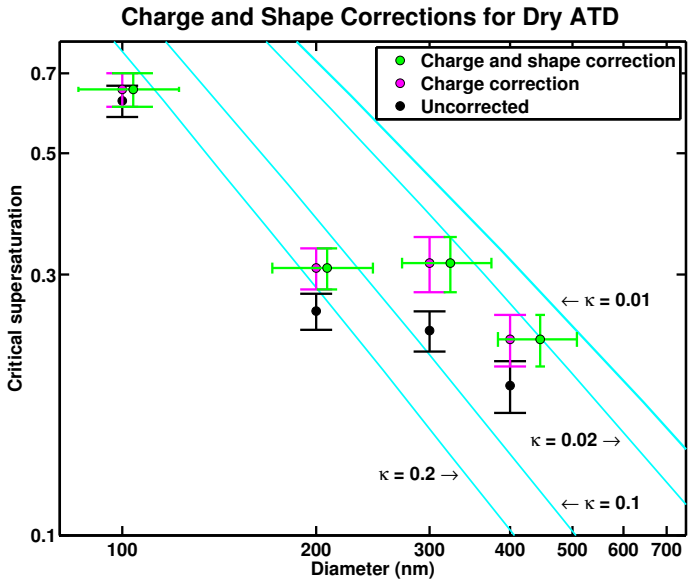

Fig. 3. Critical supersaturation as a function of size for dry-generated ATD. Raw data (black) are shown along with charge corrections (magenta), and charge and shape corrections (green). Dashed cyan curves are lines of constant κ. After shape correction, particles are classified by their surface area equivalent diameters instead of by their mobility diameters. The y-error bars indicate the standard deviation of measured supersaturation. The x-error bars indicate the range of possible values of surface area equivalent diameter.

ACPD
13, 31041–31078, 2013

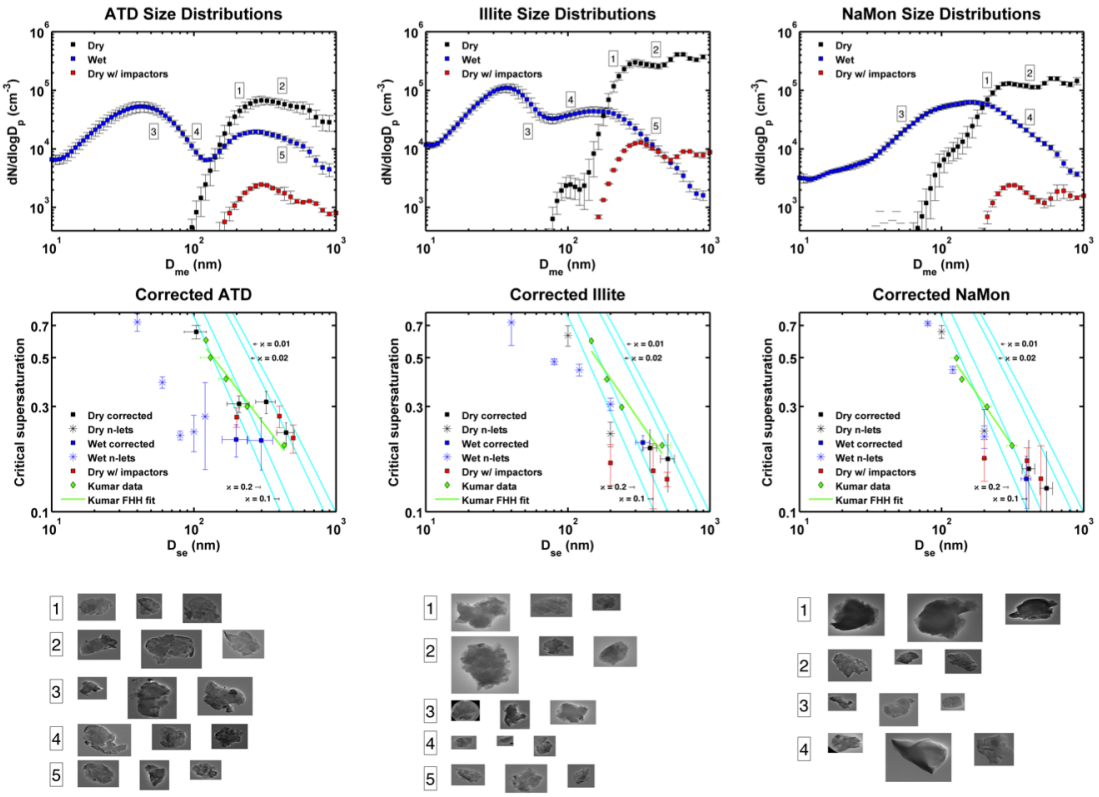

Fig. 4. Please see caption on next page.

ACPD
13, 31041–31078, 2013

CCN activity of dry- and wet-generated mineral dust aerosol

S. Garimella et al.

Fig. 4. Top row: Size distributions for the wet- (blue), dry-generated (black) samples, and cyclone-impacted dry-generated (red) samples. Boxed numbers adjacent to the blue and black distributions indicate the sizes that were analyzed with electron microscopy. Note the difference for wet and dry generation. For the swelling clays (ATD and illite) the wet-generated distributions are bimodal. For NaMon, a non-swelling clay, the wet-generated distribution is unimodal. Cyclone impaction reduces the overall concentration of particles entering the DMA and shifts the peak concentration to a smaller size. Middle row: charge and shape-corrected results form this study in blue and black, charge-corrected and cyclone-impacted data in red, lines of constant κ in cyan, and data from Kumar et al. (2011b) in green. The blue and black squares represent particle sizes for which the shape correction in this paper can be applied. The blue and black stars represent particle sizes for which the shape correction cannot be applied because only multiply charged particles with observed diameters that are integer multiples of the desired size, not singlets, are observable on the microscope grid. Bottom row: typical images from the EM analysis. The boxed numbers on the left of the images correspond to the sizes indicated in the first row of this figure.

ACPD
13, 31041–31078, 2013

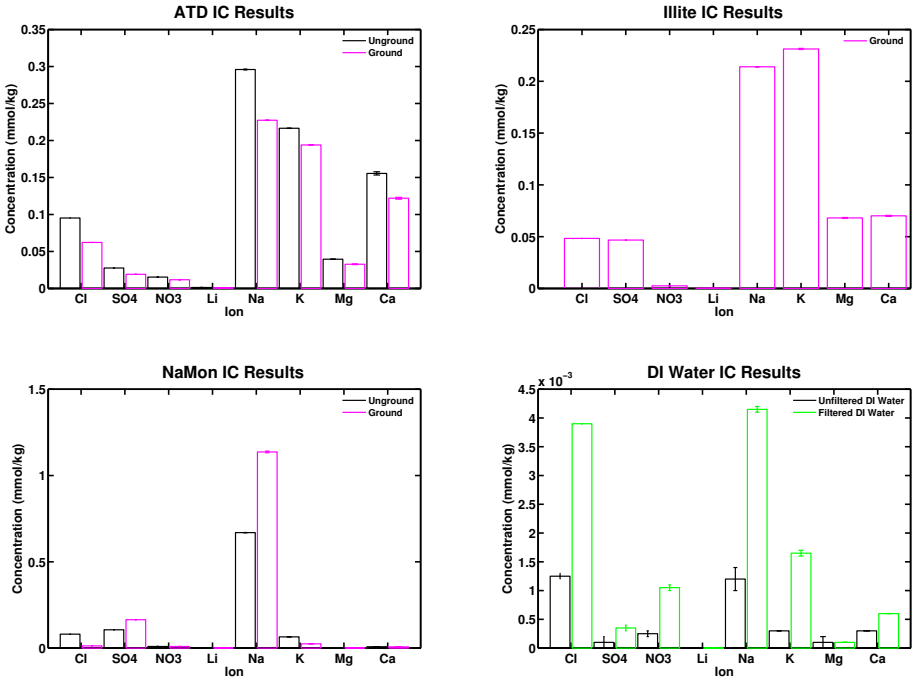

Fig. 5. Results from ion chromatography analysis for filtered supernatants of ground (magenta) and unground (black) samples of the three mineral dusts and unfiltered (black) and filtered (green) DI water control. The filtered slurry supernatants show higher concentrations of soluble material.

ACPD
13, 31041–31078, 2013

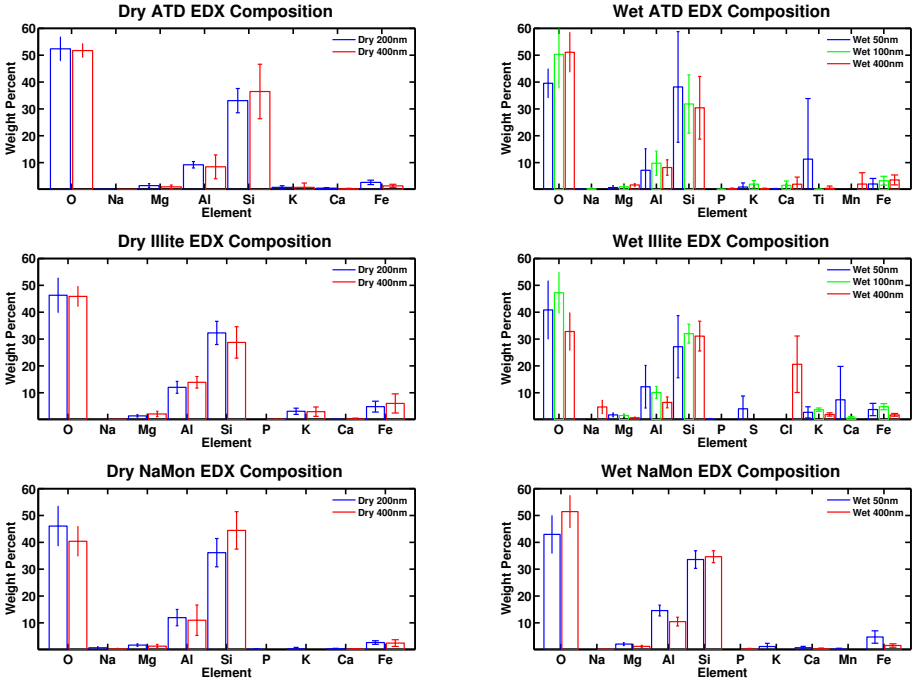

Fig. 6. Elemental abundances measured using EDX indicating minimal size dependence in the composition. The wet-generated particles (right) exhibit additional elements (red boxes on x-axis) compared to dry particles (left), which may correspond to soluble material repartitioning. Color bars indicate size according to the legend.

ACPD
13, 31041–31078, 2013

CCN activity of dry- and wet-generated mineral dust aerosol

S. Garimella et al.

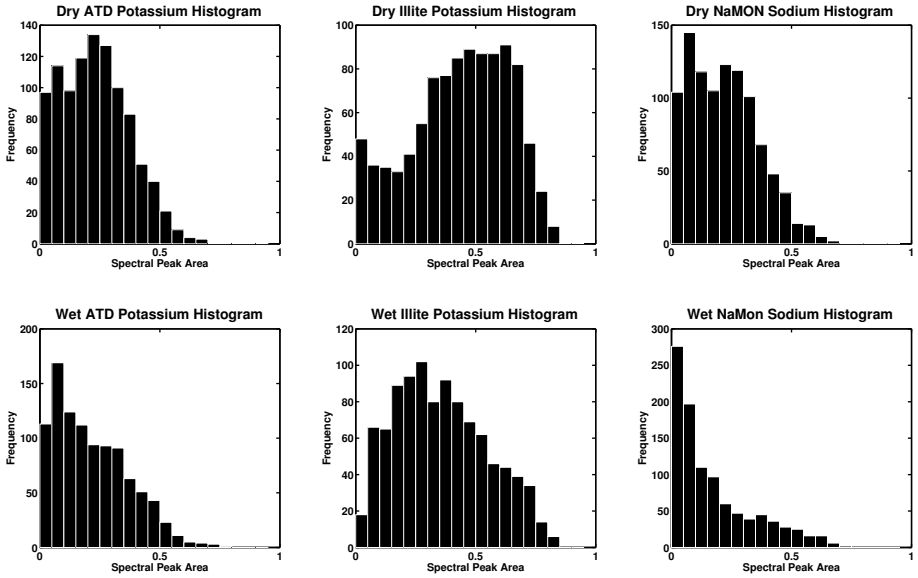

Fig. 7. Histograms showing peak areas spectra collected with PALMS. IC results (Fig. 5) show that potassium is very abundant in ATD and illite and that sodium is abundant in NaMon. Shifts toward smaller peak area (less relative abundance) can be seen in the wet-generated samples (bottom).

ACPD
13, 31041–31078, 2013

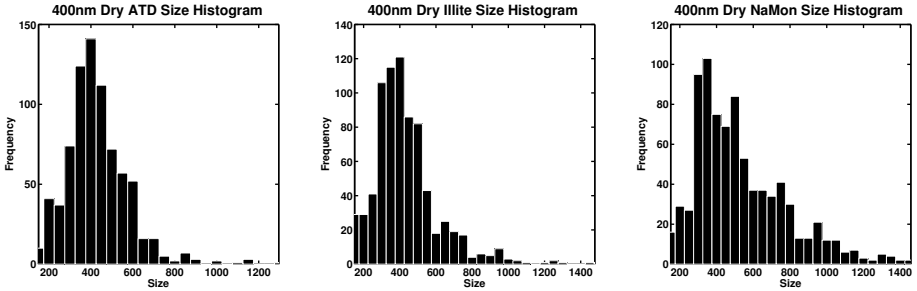

Fig. 8. Aerodynamic size distributions obtained from PALMS. Sizes are recorded downstream of the DMA, which is set to select 400 nm particles. The peaks of the distributions are at the desired size, indicating that the majority of doublets and triplets are removed. Standard charge correction procedures (Wiedensohler et al., 1988) account for the remaining large particles.

ACPD
13, 31041–31078, 2013

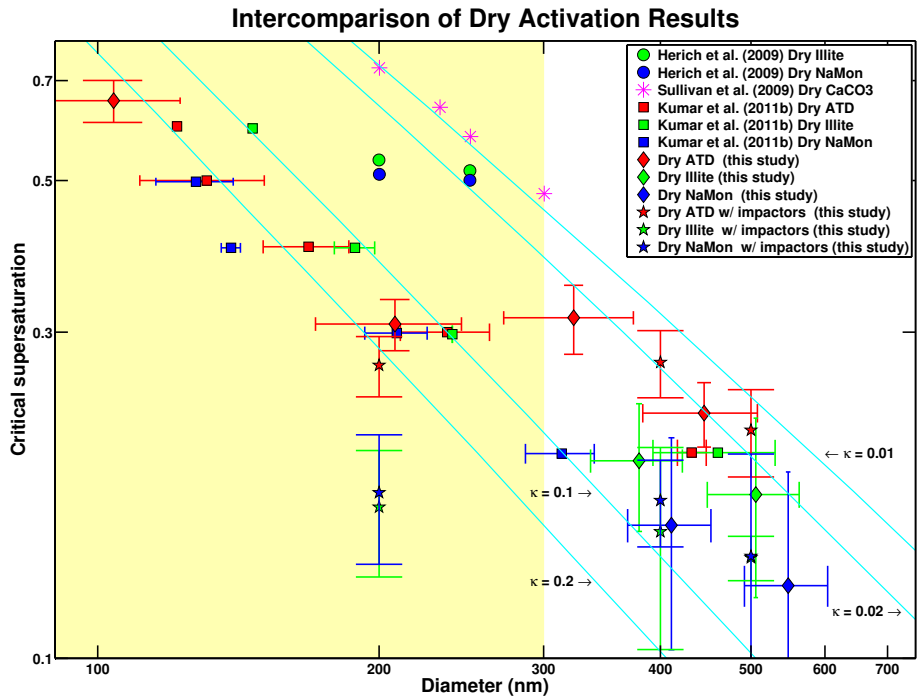

Fig. 9. Critical supersaturation vs. diameter of dry-generated particles from this study compared to results from previous studies and lines of constant κ. The data in the yellow shaded region (< 300 nm) are unlikely to be correctly sized, as indicated by the EM results.

ACPD
13, 31041–31078, 2013